Growth, perfection and properties of the organic non-linear optical crystal, 4-aminobenzophenone (ABP)

Feng Pan,† John N. Sherwood* and Graham S. Simpson‡

Department of Pure and Applied Chemistry, University of Strathclyde, Glasgow, UK G1 1XL

4-Aminobenzophenone (ABP) has been purified and grown as a single crystal using both melt and solution growth techniques. Solution growth from *N*,*N*-dimethylformamide (DMF) yielded the most perfect crystals in sizes up to $25 \times 20 \times 40$ mm. Due to the development with time of a pink impurity in DMF solutions all ABP crystals grown from DMF solution incorporated this impurity in the {001} sectors. This could be minimised by adjusting the growth conditions to reduce the development of these sectors. Investigation showed that residual quantities of this impurity in the crystals had little influence on the crystal properties.

The growth mechanism is discussed from the viewpoints of the structures of the molecule and the crystal and their relationship to the external crystal morphology. The perfection of the crystal was defined by microscopy and by section and projection X-ray topography. The relationship between the perfection of the crystal and its linear and non-linear optical performance was investigated.

Non-linear optical techniques are developing towards the goal of integrated, small-scale technology using high-intensity and broad spectrum band pass laser light. Three wavelength regions of transparency are of interest in the definition of non-linear optical (NLO) materials for frequency conversion; far-UV (<200 nm), visible (350–700 nm) and far-IR (*ca.* 10 000 nm). The far-UV and far-IR regions are well served by inorganic compounds and semiconductor compounds, respectively. A particular challenge for NLO materials is to develop a blue–violet frequency conversion material for use with small-scale and miniature semiconductor lasers (wavelength *ca.* 860 nm). Using $KNbO_3$ crystals, which exhibit the largest second-harmonic generation (SHG) effect of the inorganic crystals, 42% efficiency for the above purpose has been obtained under laboratory conditions.[1,2] The use of this material is limited however since the operational temperature range is rather narrow and must be precisely regulated. Thus, the prospect for organic NLO crystals in this application is of major interest.[3] The goal is to develop an organic crystal with an optical absorption edge in the 420 nm region and a non-resonant coefficient of the order of 10 to 50×10^{-9} esu (*i.e.* ten times the efficiency of urea).[4]

Of particular importance for this purpose are donor–acceptor conjugated molecular systems, some of which exhibit highly non-linear optical properties. For these materials non-linear efficiency varies with transparency since increasing the size of the conjugated electron system leads to a lowering of the energy of the excited state and increasing colouration. Thus, the selection of molecular types, *i.e.* the selection of the kinds of donor, acceptor and conjugated electron system, is a key point in the molecular engineering and design of organic NLO crystals for blue light. A survey of potential organic materials of this type using both theoretical and spectroscopic assessment revealed the general suitability of 4-aminobenzene-carbonyl (4-ABC) molecular types for this purpose.[5] The most promising material of this type is 4-aminobenzophenone (ABP).

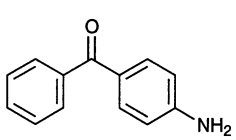

† MOEC, 877 25th Street Watervliet, New York 12189, USA.
‡ School of Chemistry, University of St. Andrews, St. Andrews, Fife, UK KY16 9ST.

Experiments with this material have demonstrated high powder second harmonic generation, *e.g.* $360 \times$ ADP,[6] $250 \times$ ADP[7] and $10 \times$ urea (this work). Hence it was of interest to select ABP as a model material to assess the reliability of the theoretical calculations of optical properties and to extend the understanding of the relationship between molecular and crystal properties. In this work ABP was purified and grown as a single crystal using both melt and solution growth techniques. The crystals have subsequently been used for a complete analysis of the linear[8] and non-linear[5] optical properties of this material.

Purification and purity

Attempts to purify reagent grade ABP (Aldrich) used the conventional methods of recrystallisation and column chromatography. ABP shows a tendency to decompose slowly in the melt over long periods of time which precludes the use of zone refining. Column chromatography using silica gel and dichloromethane followed by recrystallisation from water produced white needle-like crystals which showed no detectable impurities by DSC, spectroscopy and gas chromatography–mass spectrometry. We conclude that the purity is better than 99.9%.

The chemistry of ABP in solution has the added complication of the slow photo-oxidation[9,10] of ABP to produce a red–pink impurity, which can be incorporated into certain sectors of the final crystal. The effect of this incorporation and attempts to identify this impurity will be discussed below.

Crystal orientation

ABP forms a monoclinic crystal structure spacegroup $P2_1$ with $a = 1.2036$, $b = 0.5450$, $c = 0.8299$ nm and $\beta = 97.86°$;[11] There are two molecules per unit cell. Grown crystals were orientated by a combination of X-ray diffraction and optical goniometry.

Crystal growth from the melt

Growth from the melt was accomplished in a two-zone furnace similar to that described by McArdle *et al.*[12] The temperature gradient of $5\ °C\ cm^{-1}$ was achieved using 3-methylbutanol in the upper zone and heptane in the lower zone.

The crystal growth tube with a seeding tip was lowered through the system at $0.8\ mm\ h^{-1}$ and stirred at 10 rpm. The resulting crystal boule showed three distinct zones: a lower

(first grown) region of poor structural quality, a central region of good optical quality and an upper (last grown) region in which dark brown decomposition products had been incorporated.

The central section of the boule cleaved easily at an angle of *ca.* 30° to the growth axis to yield material of good optical quality. Subsequent Laue analysis of such cleaved samples confirmed the cleavage plate to be (100) but showed the material to be highly strained as evidenced by a considerable asterism. The mosaic spread was estimated to be *ca.* 0.8°. In general Bridgman grown material was unsuitable for optical studies.

ABP crystal growth from solution

Choice of solvent

In the growth of crystals from solution the solvent can influence the habit due to the interaction of solvent with the surfaces of the growing crystal. This is especially so for the crystal growth of highly polar molecular crystals. Table 1 shows the changes in the morphology of ABP crystallised from solvents of different polarity (expressed as their dipole moments).

From this examination methanol, ethanol and DMF were selected as suitable solvents for good growth. The first two solvents yielded crystals of a thick plate-like habit and good quality and the last prismatic crystals of good quality. These characteristics were the most promising from the viewpoint of preparing large crystals for optical and structural evaluation. In air and under normal light conditions, it was noted that the crystallisation solution changed with time from colourless to a deep-pink colour. These changes were most pronounced for the solvents toluene, ethyl acetate, acetone and chloroform. This pink colour was incorporated into the ABP crystals. As noted previously, this phenomenon was probably the consequence of the photochemical oxidation of ABP in solution. Subsequent growth experiments were carried out in the dark to minimise this effect.

Growth from methanol and ethanol solutions

The solubility curves for ABP [Fig. 1(*a*)] in both methanol and ethanol solutions were defined by saturating solutions at high temperature, cooling the solution slowly in the presence of precipitated solid to maintain equilibrium and sampling, and analysing the solution at defined temperatures. Both curves for methanol and ethanol shows a regular behaviour with solubility coefficient $(dS/dT)/S_0 = 0.04$ and $0.02\ K^{-1}$, respectively, for $T_0 = 308$ K (S is the solubility and T temperature, S_0 is the solubility at T_0). These are close to the range of $0.01–0.03\ K^{-1}$ defined empirically as satisfactory for growth by the temperature lowering method.[13]

Spontaneously nucleated crystals of ABP grew from methanol and ethanol solutions with a thick tablet-like morphology with large {001} faces. The tablet was bounded by {100} and {110} faces. The morphology of an ABP crystal grown from methanol is shown in Fig. 2(*a*).

The nature and morphology of crystals of ABP varied considerably with supersaturation σ [$\sigma = (s - s^*)/s^*$ where s is the actual solubility at a given temperature and s^* is the equilibrium solubility]. In general, the rate of growth of the {001} faces was much slower than that on {110} and {100} faces at all supersaturations. At low supersaturations (σ *ca.* 0–0.05) the growth rates in the *a* and *b* directions are almost identical. This leads to the observed plate-like morphology shown in Fig. 2(*a*) and (*b*). The growth rate on {110} faces at higher supersaturations ($\sigma > 0–0.05$) was such that rapid, unstable growth was often initiated leading to the development of surface macrosteps and the inclusion of solvent in these sectors [Fig. 2(*b*)]. This rapid growth on {110} faces if unchecked leads to a morphology extended in the *b* (polar) direction. This type of growth is typical for highly polar organic materials at relatively high supersaturations.[14]

The procedure used for large crystal development (Fig. 3) is similar to that used for the growth of MBANP.[15] Long seed crystals [Fig. 3(*a*)] were developed in methanol solution at high supersaturation to yield rapid but imperfect growth along

Table 1 The habit of ABP crystals grown from solvents of different polarities

solvent	dipole moment /10^{-30} C m	habit	visual quality
toluene	1.3	needle	poor
chloroform	3.7	tabular	poor
methanol	5.5	plate	good
ethanol	5.7	plate	good
ethyl acetate	6.2	tabular	poor
acetone	10.0	prismatic	good
DMF	12.1	prismatic	good

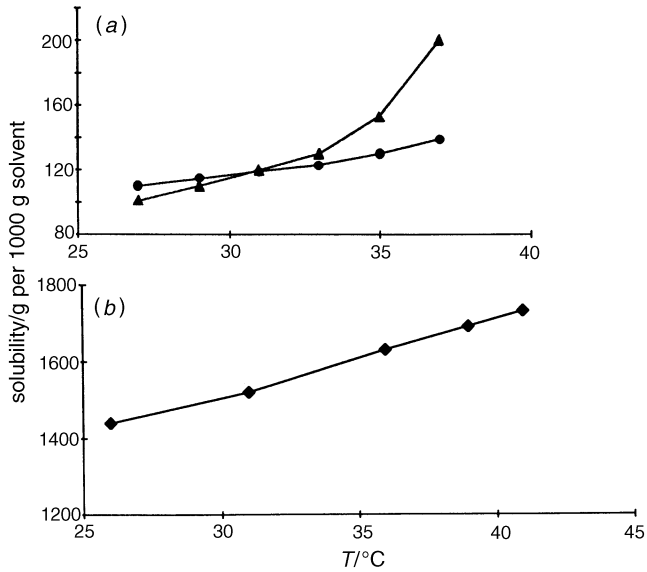

Fig. 1 The solubility curves for ABP in (*a*) (●) methanol and (▲) ethanol, (*b*) DMF

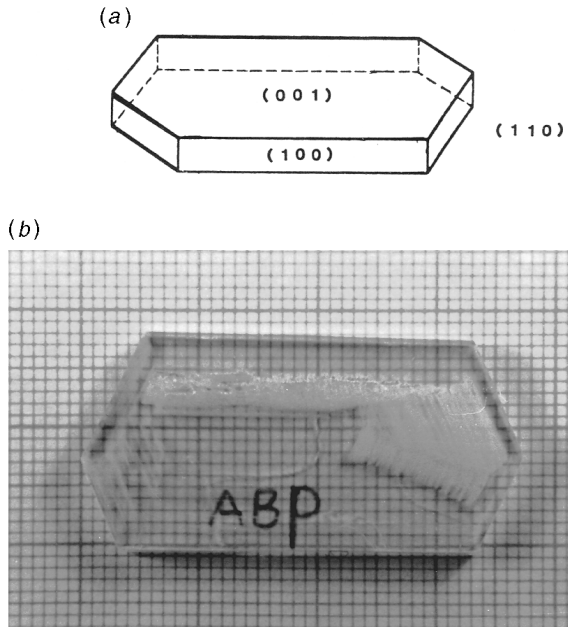

Fig. 2 The morphology of ABP crystals grown from methanol solution; (*a*) schematic, (*b*) as grown crystal (smallest scale division = 1 mm)

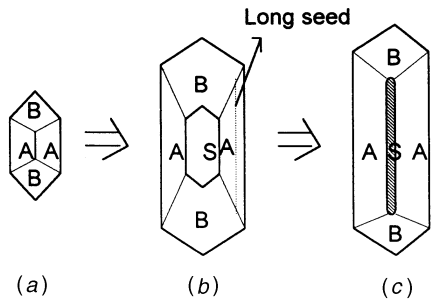

Fig. 3 A schematic diagram showing the development of elongated seeds from methanol solution

the *b* direction [Fig. 3(*b*)]. Simultaneously, the lateral {100} sectors grew well to produce narrow regions of high quality crystal. From the outermost parts of these regions long seeds were cut. These seeds were then many times longer than the initial seed crystal in the *b* direction. Repetition of this process produced successively larger seeds which when grown on at low supersaturations yielded crystals of high quality [Fig. 3(*c*)]. Fig. 2(*b*) shows an ABP crystal, $19 \times 38 \times 2$ mm ($a \times b \times c$) grown by this process. The quality of the different sectors is clearly visible. In this manner, it is relatively easy to produce large {100} volumes of high optical quality whereas only relatively small {001} and {110} volumes can be produced.

Growth from *N*,*N*-dimethylformamide (DMF) solution

DMF is a highly polar solvent in which ABP is very soluble [Fig. 1(*b*)]. On standing the solutions develop a deep-pink colour. The solubility coefficient, $(dS/dT)/S_0$, is 0.01–0.02 K^{-1} at 25–45 °C which again lies within the empirically defined region for growth by temperature lowering. Plate-like seeds of long *b* dimension were again used. The typical crystal morphology of ABP grown from DMF solution is shown in Fig. 4(*a*). The relationship between ABP growth habit and supersaturation (σ) in DMF solution can be summarised as follows.

When $\sigma > 0.01$ the growth rate of the {100} faces was slower than the {001} and {110} faces. Under such conditions the $(\bar{2}01)$ and $(20\bar{1})$ faces remained small. Fig. 4(*b*) shows an example of a crystal grown under these conditions.

In the range $0.004 < \sigma < 0.01$ the size of both the $(\bar{2}01)$ and $(20\bar{1})$ faces increased with decreasing supersaturation whilst the growth rate of the {100}, {001} and {110} faces became similar.

Finally with $\sigma < 0.004$ growth on $\{\bar{2}01\}$ became similar to that of {001} with the result that under some circumstances $\{\bar{2}01\}$ faces dominated over {001} in the habit.

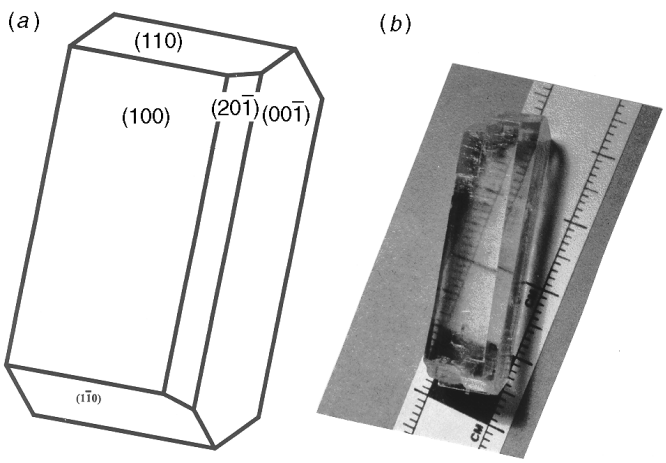

Fig. 4 The morphology of ABP crystals grown from DMF solution; (*a*) schematic, (*b*) as grown crystal (scale mark = 1 cm)

This variation is demonstrated well by the crystal sectors shown in Fig. 5(*a*), and the schematic diagram in Fig. 5(*b*). This section was cut from a crystal, $18 \times 30 \times 20$ mm ($a \times b \times c$), grown from a (100) plate seed, $0.8 \times 25 \times 10$ mm.

The development of the $(\bar{2}01)$ and $(20\bar{1})$ sectors can be seen to vary relative to (001) and $(00\bar{1})$. Interestingly, all ABP crystals grown in DMF solution show a strong degree of incorporation of the pink impurity into only the {001} growth sectors [Fig. 5(*a*)]. Both the pink and clear sections of the crystals grown are of good optical quality. Variation of supersaturation during growth can lead to morphological changes which minimise this effect. Growth in the range of supersaturation which encourages the formation of the $(\bar{2}01)$ and $(20\bar{1})$ sectors results in smaller {001} sectors and hence less material containing impurity.

In DMF solution, by using long dimensional seeds, *e.g.* $a \times b \times c = 0.5 \times 20 \times 2$ mm cleaved from crystals grown from methanol solution, larger, more prismatic ABP crystals of high optical quality could be grown with minimal impurity incorporation.

Structure of growth face and solvent effect in ABP solution growth

As noted above, the morphology, growth rate, speed and stability of growth faces of ABP crystals were influenced by variations in the types of solvents used for growth and supersaturation. It is interesting to investigate the growth mechanism from the viewpoints of the molecular structure, the crystal packing and their relationship to the external crystal shape.

The external shape of molecular crystals can be predicted by a number of methods. The Bravais–Friedel and Donnay–Harker (BFDH) analysis (Table 2) relates the morphology directly to d_{hkl}, the interplanar spacing, subject to the symmetry constraints of the space group. Those faces with the largest d_{hkl} will be the dominant morphological faces.

The periodic bond chain (PBC) analysis of Hartman and Perdok proposed that the controlling factor in the growth of crystals was the energy released on the addition of a growth slice to the surface of the growing crystal. This attachment

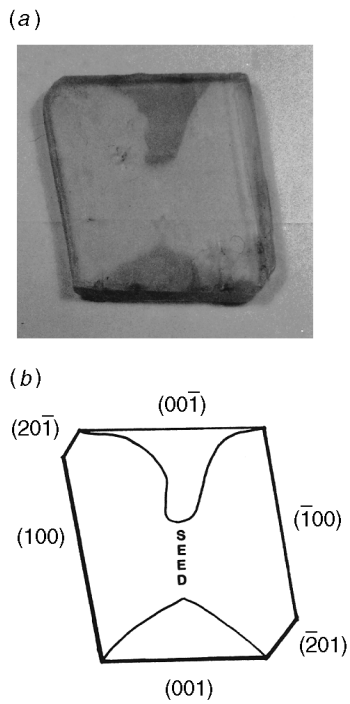

Fig. 5 (*a*) A photograph of a (010) slice of an ABP crystal grown from DMF solution showing the incorporation of the pink impurity into the {001} sectors (dark regions). (*b*) A schematic diagram showing the position of the various growth sectors.

Table 2 The morphologically important faces for ABP using the BFDH analysis

face (hkl)	multiplicity	slice thickness d_{hkl}/nm	experimentally observed
(100)	2	1.1923	yes
(001)	2	0.8221	yes
(10$\bar{1}$)	2	0.7247	no
(101)	2	0.6373	no
(20$\bar{1}$)	2	0.5174	yes
(1$\bar{1}$0)	4	0.4957	yes

energy E_{att} is directly related to the growth rate of a particular face and hence to the morphology; faces with the smallest E_{att} will have the slowest growth rates and thus will be the most important morphologically.[16,17]

It is important to remember that the morphology predicted is a growth morphology and takes no account of supersaturation.

Table 3 shows the attachment energies for the different faces of ABP.

The attachment energies, E_{att}, were calculated using the computer program HABIT 95[18] operating in full lattice mode using the X-ray structure given by Su *et al.*[11] and an intermolecular potential function combining a Lennard–Jones 6–12 potential with a 10–12 H bond potential.

Both the BFDH and the attachment energy calculations predict that {100} will be the dominant morphological face, followed by {001}. The other faces predicted by the two methods are generally in agreement although the relative order of importance differs considerably.

The role of the solvent in the inhibition of crystal growth can be understood by considering the adsorption of solvent molecules onto certain faces which must then be removed prior to incorporation of further growth units. This will place an additional energy barrier to the further growth of that particular face which will inhibit growth and result in the increased morphological importance of the face.[19]

The presence of large {001} facets in the morphology of ABP crystals grown from solvents with the potential to form hydrogen bonds such as methanol and ethanol should result from the inhibition of the growth rate of {001} faces. This can be rationalised by observing the structure as viewed along [010] (Fig. 6). It is clear that the amino groups of both molecules in the unit cell are orientated in such a way that would lead to strong hydrogen bonded interactions with methanol–ethanol molecules on the {001} surfaces. This strong interaction would slow the growth rate of such surfaces and is therefore one possible reason for the observed dominance of {001} in the final morphology. In contrast, the {100} surfaces are dominated by phenyl groups which are less likely to form hydrogen bonds with the solvent.

The difference in morphology of ABP crystals grown from DMF cannot be explained in such simple terms. The highly polar nature of the solvent and the high solubility (1500 g l^{-1} at 303 K) leads to complex solvent–solute interactions on all growing faces of the crystal. It is interesting to note the structure of both the ($\bar{2}$01) and (20$\bar{1}$) faces, the presence (or absence) of which plays such a crucial role in the incorporation of the pink impurity into the {001} sectors. Fig. 6 shows the

Table 3 E_{att} of different growth faces of ABP crystal

growth face	E_{att}/kcal mol^{-1}[a]	growth face	E_{att}/kcal mol^{-1}
(100)	−6.56	(10$\bar{2}$)	−19.09
(001)	−15.89	(210)	−20.63
(10$\bar{1}$)	−15.98	(20$\bar{1}$)	−21.37
(110)	−18.49	(101)	−21.82

[a]1 cal = 4.184 J.

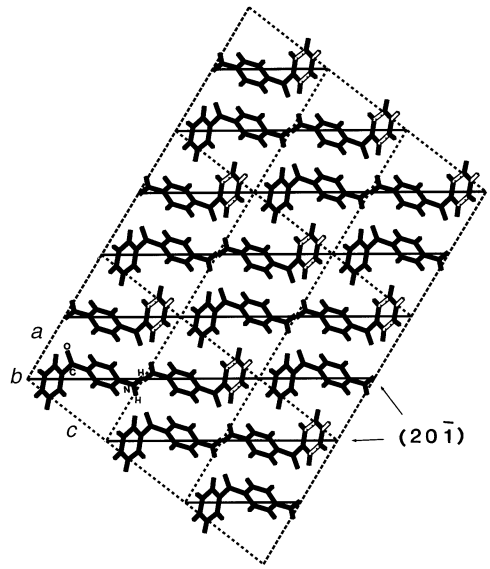

Fig. 6 The packing diagram showing the molecular arrangement of ABP on the *ac* plane looking down the *b*-axis. The (20$\bar{1}$) plane is indicated by the solid line.

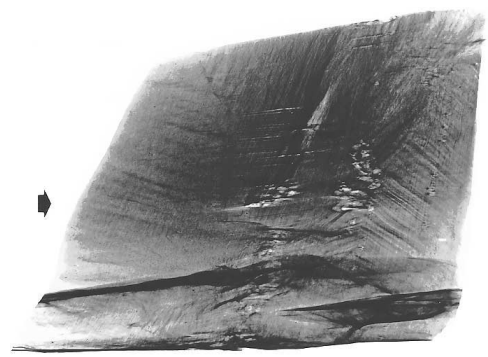

Fig. 7 A 300 projection topograph of a (010) slice of DMF grown ABP. The broad arrow indicates the *g* vector of the incident X-radiation.

structure of the (20$\bar{1}$) face. It is clear that the 'chemical nature' of this face is dominated by carbonyl groups which emerge on this surface. In contrast, the amino–phenyl–carbonyl polar direction lies in-plane thus contributing little to the polar nature of this surface but certainly influencing the adjacent {001} surfaces. Thus, both surfaces have the potential to interact with the DMF solvent molecules. The exact nature and extent of this interaction and the supersaturation dependence would determine the growth rate and hence the size of each face in the final crystal. It is not possible to rationalise this further.

X-Ray topography of solution grown crystals of ABP

The structural quality of ABP was investigated using both projection and section X-ray topography. This was carried out using station 7.6 at the Synchrotron Radiation Source in Daresbury Laboratory.

(010) slices of ABP were cut, polished and etched to produce samples of thickness 0.5–1.0 mm. This sample thickness gave a product of the mass absorption coefficient (μ) and thickness of the sample (t), μt, approximately equal to 1 which is suitable for the production of kinematical diffraction images (extinction contrast).[20]

(010) slices were investigated to allow direct comparison of the sectoral dependence of perfection with the presence of the pink impurity in the {001} sectors.

Fig. 7 shows a topograph (300 reflection, $\lambda = 1.5$ Å) from a (010) slice, within which both {001} sectors have incorporated the pink impurity. In general terms, the image shows the overall dark contrast which appears to be typical of crystals of highly polar organic materials.[15,21] The cause of such contrast is not yet clear but perhaps reflects a higher degree of lattice strain inherent in the growth of highly polar organic crystals. This overall dark contrast, coupled with the considerable deformation which has occurred during preparation, tends to obscure much of the detail. Growth sector boundaries, growth striations, solvent inclusions and dislocations (although often not individually resolved) can be readily identified.

The topograph shows well the higher degree of strain associated with the impure {001} sectors. The presence of the $\{20\bar{1}\}$ faces has limited the size of the {001} faces and hence the amount of incorporation of the impurity and the resulting strain. Overall the lack of quality of the topograph highlights the problems which occur during the preparation of the very thin projection topographic samples from such plastic materials. This can be avoided by the characterisation of uncut ABP crystals using section topography.[22]

Fig. 8(*a*) and (*c*) show synchrotron white-radiation section topographs taken through the centre of an ABP crystal grown from DMF solution. The only difference between the two topographs is that in Fig. 8(*a*) the incident beam is normal to the largest face (100) whereas in Fig. 8(*c*) the input face for the X-ray beam is (001). The images were formed predominantly from the 020 reflection at 1.2 Å and 040 at 0.6 Å with a Bragg angle of 15°. The section topography reveals detail of the growth history of crystal as well as highlighting the strain sensitivity of the technique.

On first inspection Fig. 8(*a*) seems to show an extremely distorted image from a highly strained sample. However the topograph should be considered in three separate sections [The sections are marked by dashed lines on the Fig. 8(*b*)]. The two outer sections account for almost 95% of the actual width of the image while the central, highly distorted section which contains the seed accounts for the remainder. It appears that this particular diffraction geometry is highly sensitive to the strain which is always associated with the seed–crystal boundary.

In the two outer sections, which suffer little of the image asterism associated with the central section, dislocations and growth sector boundaries can be clearly identified and in general the quality of the images in these regions confirms the high structural quality of the crystal.

The topograph shown in Fig. 8(*a*) can be contrasted with that shown in Fig. 8(*c*). This topograph was recorded under identical diffraction conditions except that the X-ray beam was incident on (001). The topograph in this case shows an image with little or no asterism. The dark contrasted areas at the top and bottom of the topograph correspond to the {001} sectors of the crystals which as previously noted incorporated the pink impurity. This dark contrast we presume is related to the strain associated with this incorporation.

Relationship between the purity and perfection of the crystal and its linear, non-linear optical and spectral properties

The linear[8] and non-linear[5] optical properties of ABP have been extensively studied and reported. It is however interesting to define the small differences which exist between the clear and pink sections of the crystal. The refractive indices of ABP have been measured by the minimum deviation technique using prisms orientated, cut and polished from DMF-grown crystals. The refractive indices n_x and n_y show no difference between the clear and pink sections. However the refractive index in the *z*-dielectric axis direction, n_z, measured in the pink sectors showed a difference of up to five times the largest error for that in the clear sectors in the wavelength region of 620–420 nm. Table 4 shows that the d_{22} and d_{23} coefficients

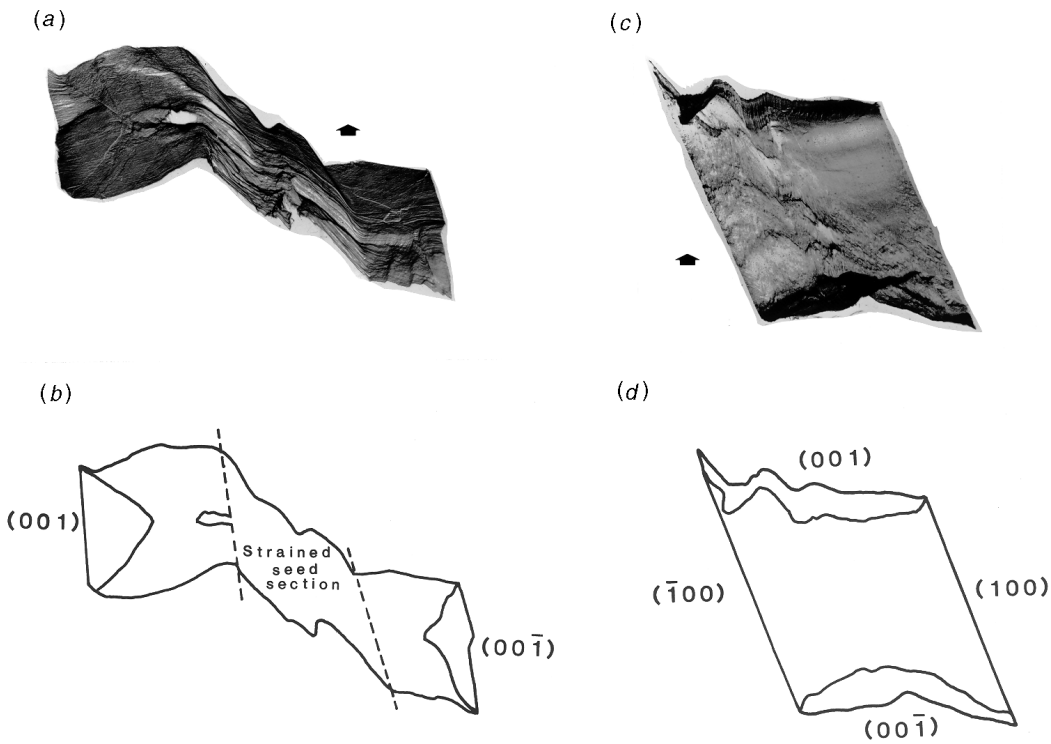

Fig. 8 0*k*0 X-Ray section topographs of an uncut ABP crystal grown from DMF solution. The input faces for topograph (*a*) and (*c*) are (100) and (001), respectively. The schematic diagrams (*b*) and (*d*) show the principal features of each topograph. The broad arrow indicates the *g* vector of the incident X-radiation.

Table 4 Comparison of the non-linear optical properties in the clear and pink sectors of ABP

	λ /nm	d_{22} /pmV^{-1}	d_{23} /pmV^{-1}	PM[a] θ_{inc}	PM SHG[b] intensity
clear	1064	1.8	21.5	29.0	310 000
pink	1064	1.7	21.1	29.0	200 000
clear	870	3.7	115	50.8	5 000 000
pink	870	3.4	112	50.8	4 000 000

[a]PM θ_{inc} is the incidence angle for phase matched second harmonic generation (SHG). [b]PM SHG intensity is the relative phase matched SHG output intensity referenced to quartz d_{11}.

and the incidence angles for phase matching are identical (within experimental error 5–10%) for both sections.

The only difference observed is the 20–30% reduction in the phase matched intensity for the pink sector. This reduction may be caused by the colouration of the section or by the increased structural imperfection associated with the incorporation of the pink impurity into the crystal. Such variations of phase matched intensities with structural imperfection have been observed for other materials.[23,24]

Absorption spectra of the two sections showed no observable distinction. However, when a polarised beam from a multiline Ar^+ ion laser (principal wavelengths 488 and 514.5 nm) was passed through both sections along the *z*-dielectric axis a yellow fluorescence emission (wavelength estimated to be 580 nm) was observed only from the pink section. At the present time, it has not proved possible to identify the structure and/or the orientation of the species responsible for the fluorescent emission. In summary, the pink impurity which only incorporates into the {001} sectors has only a marginal effect on the intrinsic optical properties of ABP.

This programme of work was supported by the EPSRC and the US Naval Research Laboratory. F. P. thanks the CVCP ORS Scheme, and the University of Strathclyde for the provision of tuition fees and a maintenance grant. The provision of beamtime at Daresbury Laboratory is also acknowledged. Our sincere thanks are due to Mrs E. Shepherd for helping in the growth of crystals from solution and in the cutting and polishing of the crystals.

References

1 M. K. Chun, L. Goldberg and J. F. Weller, *Appl. Phys. Letts*., 1988, **53**, 117.
2 L. Goldberg, *Appl. Phys. Letts*., 1989, **55**, 218.
3 J. Zyss, *J. Phys. D*., 1993, **26**, B198.
4 J. F. Nicoud and R. J. Twieg, *Nonlinear Optical Properties of Organic Molecules and Crystals*, *Vol. I*, ed. D.S. Chemla and J. Zyss, 1987, Academic Press, Orlando, FL., p. 257.
5 F. Pan, PhD Thesis, *Design, Growth, Perfection and Properties of Organic Nonlinear Optic Crystals For Blue Light*, University of Strathclyde, UK, 1994.
6 C. C. Frazier and M. P. Cockerham, *J. Opt. Soc. Am*., 1987, **B4**, 1901.
7 G. B. Su, S. W. Guo, F. Pan, Y-P He and Z-D. Li, *J. Phys. D*., 1993, **26**, B236.
8 F. Pan, R. T. Bailey, F. R. Cruickshank, D. Pugh, J. N. Sherwood, G. S. Simpson and S. Wilkie, *J. Appl. Phys*., 1996, **80**, 4649.
9 S. G. Cohen and J. I. Cohen, *J. Phys. Chem*., 1968, **72**, 3782.
10 S. G. Cohen, M. D. Saltzman and J. B. Guttenplan, *Tetrahedron Lett*., 1969, **49**, 4321.
11 G. Su, Z. Li, F. Pan and Y. He, *Cryst. Res. Technol*, 1992, **5**, 589.
12 B. J. McArdle, J. N. Sherwood and A. C. Damask, *J. Crystal Growth*, 1974, **22**, 193.
13 B. J. McArdle and J. N. Sherwood, in *Advanced Crystal Growth*, ed. P. M. Dryburgh, B. Cockayne and K. G. Barraclough, Prentice-Hall, New York, 1987, p. 179.
14 A. F. Wells, *Disc. Farad. Soc*., 1949, **5**, 197.
15 P. J. Halfpenny, H. Morrison, R. I. Ristic, E. E. A. Shepherd, J. N. Sherwood, G. S. Simpson and C. S. Yoon, *Proc. R. Soc. Lond. A*, 1993, **440**, 683.
16 Z. Berkovitch-Yellin, *J. Am. Chem. Soc*., 1985, **107**, 8239.
17 G. Clydesdale, R. Docherty and K. J. Roberts, *Comp. Phys. Commun*., 1991, **64**, 311.
18 G. Clydesdale, R. Docherty and K. J. Roberts, *Quantum Chem. Prog. Exchange*, 1996, **16**, 1.
19 F. C. Wireko, L. J. W. Shimon, Z. Berkovitch-Yellin, M. Lahav and L. Leiserowitz, *J. Phys. Chem*., 1987, **91**, 471.
20 B. K. Tanner, *X-ray Diffraction Topography*, Pergamon Press, Oxford, 1976.
21 E. E. A. Shepherd, J. N. Sherwood, G. S. Simpson and C. S. Yoon, *J. Crystal Growth*, 1991, **113**, 360.
22 P. J. Halfpenny and J. N. Sherwood, *Phil. Magn. Lett*., 1990, **62**, 1.
23 R. T. Bailey, F. R. Cruickshank, D. Pugh and J. N. Sherwood, *Int. J. Optoelectron*., 1990, **5**, 89.
24 P. Andreazza, F. Lefaucheux, M. C. Robert, D. Josse and J. Zyss, *J. Appl. Phys*., 1990, **68**, 8.

Paper 7/00430C; *Received* 20*th January*, 1997